Title: Multispecies reactive transport modelling of electrokinetic remediation of harbour sediments

Author: Matteo Masi Alessio Ceccarini Renato Iannelli

PII: S0304-3894(16)31174-8
DOI: http://dx.doi.org/doi:10.1016/j.jhazmat.2016.12.032
Reference: HAZMAT 18264

To appear in: *Journal of Hazardous Materials*

Received date: 28-7-2016
Revised date: 2-12-2016
Accepted date: 18-12-2016

Please cite this article as: Matteo Masi, Alessio Ceccarini, Renato Iannelli, Multispecies reactive transport modelling of electrokinetic remediation of harbour sediments, Journal of Hazardous Materials http://dx.doi.org/10.1016/j.jhazmat.2016.12.032

Multispecies reactive transport modelling of electrokinetic remediation of harbour sediments

Matteo Masi*

Department of Energy, Systems, Territory, and Construction Engineering

University of Pisa

Via C.F. Gabba, 22

56122 Pisa (PI), Italy

*Corresponding author, email: m.masi@ing.unipi.it

Alessio Ceccarini

Department of Chemistry and Industrial Chemistry

University of Pisa

Via Giuseppe Moruzzi, 13

56124 Pisa (PI)

email: alessio.ceccarini@unipi.it

Renato Iannelli

Department of Energy, Systems, Territory and Construction Engineering

University of Pisa

Via C.F. Gabba, 22

56122 Pisa (PI), Italy

Tel. +39 050 2217 718

email: r.iannelli@ing.unipi.it

Graphical abstract

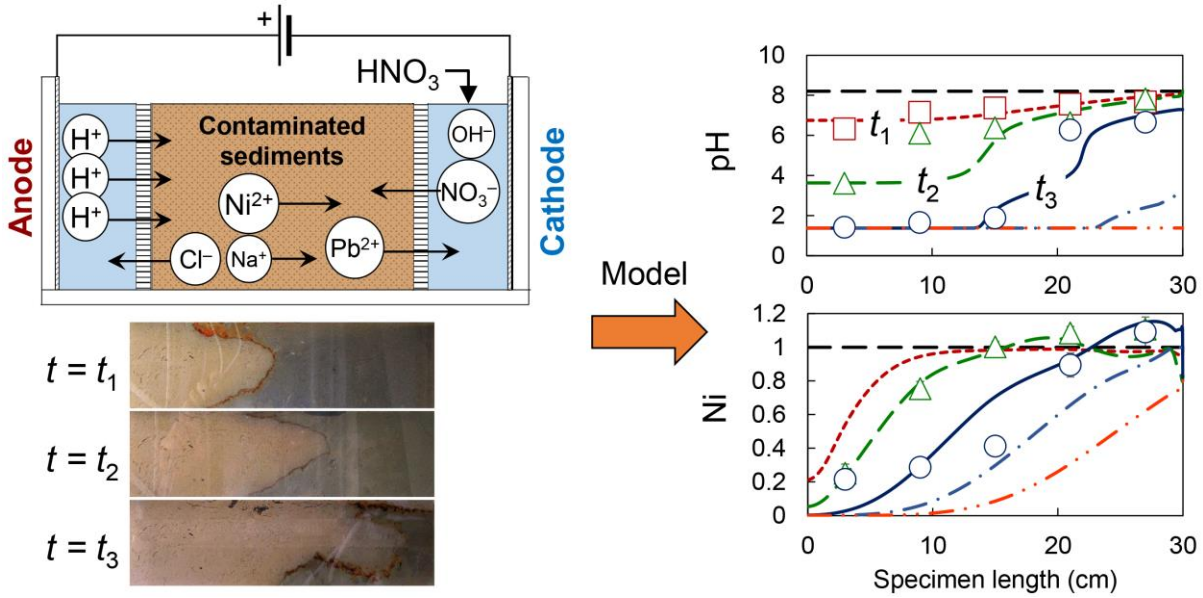

Highlights

- Electrokinetic treatment of marine sediments requires long remediation times
- Geochemical reactions have strong impact on electrokinetic transport
- Numerical model describes electrokinetic transport and reactions
- Model combining mechanistic and empirical approaches can be used for plant design

Abstract

We implemented a numerical model to simulate transport of multiple species and geochemical reactions occurring during electrokinetic remediation of metal-contaminated porous media. The main phenomena described by the model were: (1) species transport by diffusion, electromigration and electroosmosis, (2) pH-dependent buffering of H^+, (3) adsorption of metals onto particle surfaces, (4) aqueous speciation, (5) formation and dissolution of solid precipitates. The model was applied to simulate the electrokinetic extraction of heavy metals (Pb, Zn and Ni) from marine harbour sediments, characterized by

a heterogeneous solid matrix, high buffering capacity and aged pollution. A good agreement was found between simulations of pH, electroosmotic flow and experimental results. The predicted residual metal concentrations in the sediment were also close to experimental profiles for all of the investigated metals. Some removal overestimation was observed in the regions close to the anode, possibly due to the significant metal content bound to residual fraction.

Keywords: electroremediation; numerical model; heavy metals; dredged sediments; buffering capacity

1. Introduction

Harbour sediments are frequently polluted by a wide variety of contaminants accumulated during decades of human activities happening in the harbours or transported from upstream sources. Electrokinetic remediation (EKR) has been successfully employed for the treatment of sediments with low hydraulic permeability, high salinity and strong acid-neutralizing capacity due to high presence of organics and carbonates [1–6]. This technique relies on applying a low-intensity electric field which mobilizes contaminants and water through the porous medium toward the electrodes due to three main transport mechanisms: electromigration, electroosmosis and electrophoresis. The application of an electric field also induces other complex effects such as pH changes, electrode reactions and geochemical reactions [7]. Moreover, water electrolysis occurring at the electrodes generates hydroxides at the cathode and hydrogen ions at the anode, which are transported by the electric field toward the oppositely charged electrodes, determining acid and alkaline fronts moving in opposite directions. While the acid front is generally favorable for contaminant desorption from the solid matrix, the alkaline front can cause precipitation, thus hindering contaminant transport. To prevent this drawback, chemical reagents (such as weak or strong acids) can be added to the catholyte [8].

In some cases, the effects induced by electric field are not fully understood and their prediction is not achievable merely on an experimental basis. Complexity is mostly due to the

high non-linearity and transient geochemistry developing during remediation [9]. Especially in presence of sediments with high buffering and sorption capacity, remediation times of several months can be required to reach the target clean-up levels. In such cases, the prescribed laboratory experiments can get excessively time consuming for the design of full-scale implementations, and modelling could become a necessary tool to assess the main remediation parameters and predict the achievable results.

Several mathematical models have been developed to predict electrokinetic extraction of contaminants [10–18]. Most of them couple the Nernst-Planck equations with auxiliary electrical neutrality equations or with the Poisson equation of electrostatics accounting for the locally induced electrical potential due to the charge unbalance produced when ions migrate with different rates.

However, most of the models developed so far show poor agreement with experimental data. Despite the proper definition of transport processes, several models do not accurately account for species geochemistry and interactions between with the porous material such as adsorption/desorption or precipitation/dissolution, which are indeed key factor for accurate electrokinetic modelling [19]. To overcome these limits, Al-Hamdan and Reddy [20] completed the transport model with a custom sub-routine calculating chemical speciation, precipitation-dissolution, oxidation-reduction and adsorption-desorption processes. They overall observed a good agreement with experimental results for cationic metals. However, they used an artificially spiked matrix for model validation, thus neglecting the additional aging effects and heterogeneity occurring in actual contaminated materials.

Mascia et al. [21] also integrated geochemical effects in their model. They represented the interaction with the solid matrix using a two-site geochemical model taking into account ion exchange and surface complexation. They obtained an excellent agreement with validation data, but their calibration and validation were again performed with an artificially spiked matrix (commercial kaolinite clay).

Paz-Garcia et al. [11] developed a generalized model which couples transport processes (electromigration, electroosmosis, diffusion and advection) with a complete geochemical reaction framework (aqueous equilibrium, sorption, precipitation and dissolution). The unsatisfactory field-scale validation suggested that a careful representation of physicochemical processes is needed to predict electrokinetic extraction of contaminants in real situations.

Most models were developed for soils having limited buffering and sorption capacity. Modelling of electrokinetic remediation of high buffering capacity real contaminated marine sediments was not addressed so far. To overcome the limits of previous models and to readily use the model as an analysis and design tool for field scale implementation, we propose a modelling approach combining mechanistic and empirical approaches toward the description of these phenomena.

We present a one-dimensional reactive transport model based on the Nernst-Planck equations coupled with a geochemical model. The model describes species transport driven by diffusion, electromigration and electroosmosis, as well as the effect of surface reactions, precipitation and dissolution, speciation of chemical species and their interaction. To overcome the limited flexibility of current models, the widely validated full geochemical framework PHREEQC [22] was used with least possible number of additional reactions and model parameters. Particular focus was given to sediment buffering capacity to better represent the behavior of real contaminated sediments. After calibration, the numerical model was validated by comparison with experimental data.

2. Materials and methods

2.1. Governing equations

We considered diffusion, electromigration and electroosmosis as the main transport mechanisms. Electrophoresis was neglected, since colloid migration is hindered by the immobile phase of the porous medium [23]. The low hydraulic permeability enabled also to neglect advective flow because of its lower order of magnitude compared to electroosmotic flow. Moreover, we assumed that the porous medium is saturated, isotropic and isothermal; the grains are non-conductive and their surface conductivity is negligible; the osmotic effect related to concentrations gradients and streaming electrical current due to pore water flow are negligible; the pore geometry characteristics (e.g. porosity, tortuosity) do not change over time.

Under these assumptions, the flux density per unit cross-sectional area of porous medium J_i (mol m^{-2} s^{-1}) of a dissolved chemical species *i* can be expressed as [24]:

$$J_i = -D_i^* \nabla c_i - U_i^* c_i \nabla \phi - k_{eo} c_i \nabla \phi \quad (1)$$

where D_i^* ($m^2\ s^{-1}$) is the effective diffusion coefficient of the i-th specie, c_i (mol m^{-3}) the concentration of the i-th specie, U_i^* ($m^2\ s^{-1}\ V^{-1}$) the effective ion mobility, ϕ (V) the electric potential and k_{eo} ($m^2\ V^{-1}\ s^{-1}$) the coefficient of electroosmotic permeability. Due to the tortuous path of ions in the porous matrix, the effective diffusion coefficient and effective ion mobility used in Equation (1) take into account the effect of porosity n and tortuosity τ [25] and they may be defined as:

$$D_i^* = n\tau D_i \tag{2}$$

$$U_i^* = n\tau U_i \tag{3}$$

where D_i ($m^2\ s^{-1}$) and U_i ($m^2\ s^{-1}\ V^{-1}$) are the diffusion coefficient and ion mobility at infinite dilution, respectively. The tortuosity factor τ may span in the range 0.01 - 0.84 [24] depending on characteristics of the porous medium.

Diffusivity and ionic mobility can be related to a single property by the Nernst-Townsend-Einstein relation [24]:

$$U_i^* = \frac{D_i^* z_i F}{RT} \tag{4}$$

where R (8.314 J K^{-1} mol^{-1}) is the universal gas constant, T (K) the absolute temperature and F (96485 C mol^{-1}) the Faraday's constant.

Applying the law of mass conservation to Equation (1), the mass transport of the *i-th* species is given by the Nernst-Planck equation:

$$n\frac{\partial c_i}{\partial t} = -\nabla \cdot \left[-D_i^* \nabla c_i - (U_i^* + k_{eo}) c_i \nabla \phi \right] + nR_i \tag{5}$$

where R_i (mol $m^{-3}\ s^{-1}$) represents a volumetric net source or sink of c_i due to chemical reactions.

The coefficient of electroosmotic permeability k_{eo} in Equations (1) and (5) is a space and time dependent quantity. According to Hemlholtz-Smoluchowski theory, it can be related to zeta potential ζ (V) and the dielectric constant ε (F m^{-1}) and viscosity η (N s m^{-2}) of the fluid [26]:

$$k_{eo} = -\frac{\varepsilon \zeta}{\eta} n\tau \tag{6}$$

where the minus sign indicates that negatively charged particles produce an electroosmotic flow directed from anode to cathode. The tortuosity and porosity terms in Equation (6) were introduced by Casagrande [27] to include the porous matrix effects in the original Hemlholtz-Smoluchowski formulation.

Zeta potential is a function of pH and ionic strength of the electrolyte. For minor changes in ionic strength, a relationship between zeta potential and pH can suffice for prediction. We adopted a generic exponential relationship, proposed by Eykholt and Daniel [26] and used in several studies [13,28]:

$$\zeta(mV) = a + b\exp(c \cdot \mathrm{pH}) \tag{7}$$

where *a*, *b* and *c* are three empirical parameters.

Since zeta potential cannot be uniform throughout the specimen due to changing pH, we calculated the bulk electroosmotic flow rate by volume averaging the electroosmotic permeability. In the 1D case, zeta potential and electric field were assumed to vary only along the x-direction by the expression of volume-averaged electroosmotic flow $\bar{Q}_{eo,x}$ ($m^3\ s^{-1}$):

$$\bar{Q}_{eo,x} = -\frac{A\varepsilon}{\eta L} n\tau \int_0^L \zeta E_x \, dx \tag{8}$$

where A (m^2) is the cross-sectional area, L (m) is the specimen length and $E_x = -\partial\phi / \partial x$ (V m^{-1}) is the electric field in the x-direction.

2.2. Chemical reactions

Among the wide set of possible reactions, we considered only the main phenomena which most experiments recognized as main contributors to the decontamination of saline sediments. Specifically, the reactions included in the model were: (1) electrolysis of water at the electrodes, (2) pH-dependent adsorption/desorption of H^+ onto the sediment solid matrix, (3) adsorption/desorption of contaminants, (4) aqueous speciation (i.e. formation of complexes), (5) precipitation/dissolution of species.

The first set of reactions occur at the electrodes, where water electrolysis takes place:

$$2H_2O \rightarrow O_2(g) + 4H^+ + 4e^- \quad \text{(anode)} \tag{9}$$

$$2H_2O + 2e^- \rightarrow H_2(g) + 2OH^- \quad \text{(cathode)} \tag{10}$$

At the anode, the presence of Cl^- ions results in their oxidation with generation of Cl_2 gas, which compete with water oxidation. This reaction, which occurs at the beginning of treatment due to high Cl^- concentration in the pore water, was experimentally found to be short compared to the overall treatment duration [4]. Therefore, it was neglected in the model.

The acid-buffering capacity of sediments was modelled as a generalized surface complexation reaction [29,30]. Surface sites were represented by a certain amount of active sites ≡SOH, where S is a metal associated to the solid structure and located at the solid-liquid interface. Depending on electrolyte pH, these groups are subjected to protonation and deprotonation reactions according to [31]:

$$\equiv SOH + H^+ \rightleftharpoons \equiv SOH_2^+ \tag{11}$$

$$\equiv SOH \rightleftharpoons \equiv SO^- + H^+ \tag{12}$$

In the present case, a non-electrostatic model (i.e. without explicit correction for electrostatic attraction or repulsion due to the electric double-layer) was chosen to simulate protonation and deprotonation reactions. The equilibrium constants for these reactions are:

$$K_1 = \frac{[\equiv SOH_2^+]}{[\equiv SOH][H^+]}, \quad K_2 = \frac{[\equiv SO^-][H^+]}{[\equiv SOH]} \tag{13}$$

The mass action equations (13) provide a description of the macroscopic pH dependence of H^+ adsorption. However, they are not intended to accurately represent the stoichiometry of reactions at the molecular scale [32].

The adsorption of heavy metals (Pb, Ni and Zn) onto particle surfaces was modelled as an adsorption isotherm:

$$S_i^a = K_{d,i} c_i \tag{14}$$

where S_i^a (mol kg^{-1}) is the concentration of metal adsorbed onto the solid phase, $K_{d,i}$ (m^3 kg^{-1}) is a linear distribution coefficient between the liquid and solid phases and c_i (mol m^{-3}) is the concentration of the metal in solution.

The aqueous formation of complexes, precipitation and dissolution reactions were also included and their calculation was performed by the PHREEQC code using the equilibrium constants present in its thermodynamic database. Equations representing these processes are reported in Parkhurst and Appelo [33].

2.3. Numerical implementation

The transport rate for diffusion, electromigration and electroosmosis were assumed to be much slower than chemical reaction rates. From a numerical perspective, reactions can be considered fast enough to reach their equilibrium at each time interval of the numerical integration. This assumption considerably simplified the numerical implementation, allowing us to calculate transport and reactions in two separate integration steps. Several studies adopting this assumption showed good agreement with experimental data [10,20,34,35].

The structure of numerical implementation is shown in Figure 1. Transport processes and chemical reactions are implemented using a two-step sequential non-iterative split-operator scheme [36]. After initialization and setup of initial and boundary conditions of transport and reaction modules, the main loop is executed.

In a first step, diffusion, electromigration and electroosmosis are computed using COMSOL Multiphysics® [37], which solves the non-linear system of partial differential equations (Nernst-Planck equations). Equation 5, 7 and 8 are implemented herein.

In a second step, chemical reactions are calculated in PHREEQC. COMSOL and PHREEQC are coupled in the MATLAB environment using PhreeqcRM, a software module designed specifically to perform equilibrium and kinetic reaction calculations for reactive transport simulators that use an operator-splitting approach [38]. The length of the coupling step, i.e. the time interval between transport and reaction, is set by the user according to the specific case. The internal time step is automatically adjusted by COMSOL to achieve convergence.

2.4. Experimental procedure

Laboratory electrokinetic experiments were carried out to validate the model. The experiments were performed in order to assess migration behavior and removal of Pb, Zn and Ni from dredged marine sediments.

2.4.1. Sediment characterization and analytical methods

Sediments were sampled from seabottom surface layer (approx. 0-50 cm) of the Port of Livorno (Italy), using a Van Veen-like manual grab sampler. The collected material (0.3 m^3) was gathered in a tank and homogenized with a mechanical stirrer.

The particle size distribution was determined by sieve analysis and aerometry. Sediment classification was carried out according to ISO 14688-1:2002. The hydraulic conductivity was estimated by oedometric test. Sediment electrical resistivity was determined with 4-electrode method in a cylindrical sample holder.

The pH of treated and untreated samples was measured according to ISO 10390:2005. The acid buffering capacity of sediments was determined by titration method using 0.1 M HCl. TOC was measured according to the standard methods prescribed by the Italian Ministry of Agriculture and Forests. CEC was determined according to ISO 11260:1994 method.

Metal content was determined with ICP-OES after acid digestion in accordance to US EPA 3050b 1996 and US EPA 7000b 2007 methods. Metal speciation was determined through a three-step sequential extraction according to the procedure recommended by the Standards, measurements and Testing (former BCR) Programme of the European Commission. pH and heavy metal analysis and speciation procedures were applied at least to three replicates. The physicochemical properties of the sediments are presented in Table 1. The results of heavy metal speciation of untreated sediments are reported in Table 2.

2.4.2. Experimental setup and electrokinetic tests

The setup for electrokinetic tests consisted in an acrylic cell (Figure 2), composed of six parts: sediment compartment, electrode compartments, water and acid reservoirs, electrolyte overflow reservoirs, power supply and pH control system. The specimen dimensions were 30x7x7 cm. To separate sediments from electrode compartments, a nylon grid (mesh size 2 mm) and filter paper were used. The sediment was layered in the cell, statically compacted by applying 40 g/cm^2 for 24 h, and left in the cell for 3 days before starting the tests. Constant

volumes of anolyte and catholyte were kept in dedicated free-surface chambers. The electrodes consisted of a titanium mesh with a Mixed Metal Oxide (MMO) coating. An array of six graphite rod electrodes (6 mm diameter) was placed to monitor voltage drop across the sediment. Catholyte pH was monitored throughout the experiments and kept constant by nitric acid addition. Deionized water was added in both electrode chambers at a constant rate to compensate water losses for electrolysis and evaporation. Electroosmotic flow was calculated from mass balance by measuring volume changes in electrolyte overflows. Applied voltage, current and local voltage drops were continuously recorded by a data logger. Local resistivity was computed from local voltage drops as described in Masi et al. [39]. After each experiment, the material was divided into five samples and analyzed for pH and metal content.

Three experiments (EXP1, EXP2 and EXP3) were carried out applying a constant current of 40 A/m^2 for 32, 63 and 120 days. EXP 2 was previously carried out and results are taken from our previous work [4]. Nitric acid was added at the cathode to maintain a constant pH of 3. Experimental conditions are summarized in Table 3.

3. Results and discussion

3.1. Model setup and implementation

The experimental conditions were simulated by a 1D closed domain having 30 cm length, with left and right endpoints representing the electrodes, where boundary conditions were defined. The domain was discretized into 222 finite elements with individual length varying from 10^{-3} mm at the edges to 4 mm at the center of the domain. The time interval between transport and reaction steps was set to 7 hours.

The reactive transport of 21 species was modelled: H^+, OH^-, Na^+, Cl^-, NO_3^-, Pb^{2+}, $PbCl^+$, $PbCl_3^-$, $PbCl_4^{2-}$, $PbCl_2$, $PbNO_3^+$, $Pb(NO_3)_2$, Zn^{2+}, $ZnCl^+$, $ZnCl_3^-$, $ZnCl_4^{2-}$, $ZnCl_2$, $ZnNO_3^+$,

Ni^{2+}, $NiCl^{+}$, $NiNO_3^{+}$. They were chosen as those having significant concentrations at working condition (ionic composition and pH), according to preliminary PHREEQC simulations.

The diffusion coefficients of each species were taken from literature [40,41]. The complexes were assigned the same diffusion coefficients as their metal constituents. The values are reported in Table 4.

The solid phases which possibly occur under the encountered conditions were selected and included in the model with analogous criteria: $Pb_3(OH)_2(CO_3)_2$, $Ni(OH)_2$ and $Zn(OH)_2$. All equilibrium constants for solution speciation and solid phase reactions were assumed from the thermodynamic database 'minteq.v4.dat', which is distributed with PHREEQC, adapted from Allison et al. [42].

The assumed initial conditions are reported in Table 5. Initial concentrations of all complexes were set to zero.

Boundary conditions were set by taking into account species mass balances in the electrolytic chambers. Both anodic and cathodic compartments were considered as continuous flow stirred-tank reactors (CSTR), with electrochemical reactions occurring at electrode surfaces. Consequently, the boundary conditions were defined by applying the mass conservation equation to each chamber. The concentration of the i-th species inside each chamber was assumed uniform, thus the mass balances may be written as:

$$\begin{cases} V_a \dfrac{dc_i^a}{dt} = -J_i A - Q_{f,a} c_i^a + R_i^a \quad \text{(Anolyte)} \\ V_c \dfrac{dc_i^c}{dt} = J_i A - Q_{f,c} c_i^c + R_i^c \quad \text{(Catholyte)} \end{cases} \tag{15}$$

where V_a (m^3) and V_c (m^3) denote the anolyte and catholyte chamber volume respectively, c_i^a (mol m^{-3}) and c_i^c (mol m^{-3}) the species concentration in the anolyte and catholyte, J_i (mol m^{-2} s^{-1}) the flux of the i-th species (Equation 1), A (m^2) the cross-sectional area, $Q_{f,a}$ (m^3/s) and $Q_{f,c}$ (m^3/s) the anolyte and catholyte flushing flow rates (addition of deionised water at the electrode compartments), R_i^a (mol s^{-1}) and R_i^c (mol s^{-1}) the net production of the i-th species due to electrochemical reactions at the anode and cathode, respectively.

As an approximation, the species flux due to the electroosmotic flow was considered in the flux term J_i, while the electroosmotic water inflow and outflow were assumed to be negligible, because of their smaller order of magnitude compared to electrolyte flushing flow rate Q_f in the present case (approximately 400 ml/day each chamber).

We considered water electrolysis as being the main reaction occurring at the electrodes. We adopted the simplifying assumption that oxidation of chlorides at the anode could be neglected. We also considered negligible any possible electrodeposition of metals at the cathode. Consequently, assuming 100% Faraday efficiency for water at the electrodes, the reaction rate of H^+ at the anode is $R^a_{H+} = I/F$, where I (A) denotes the electric current. At the cathode, the flux of NO_3^- was considered, due to nitric acid addition, i.e., $R^c_{NO3-} = I/F$. The rates of HNO_3 addition and OH^- production at the cathode were considered equal, hence neglecting possible ammonium formation. At the cathode, the H^+ concentration was set fixed to 10^{-3} M because the pH was maintained at pH = 3 by HNO_3 addition.

3.2. Calibration of model parameters

Model parameters were either derived from literature or calibrated through laboratory batch tests or electrokinetic tests. Data used for model calibration and validation were distinct. Table 6 summarizes the parameters adopted in the numerical model. The tortuosity factor was derived from literature [18]. The porosity was experimentally determined. Batch titration tests were performed to obtain the equilibrium constants of surface complexation model (Equation 13). The constants K_1 and K_2 were adjusted to fit experimental titration data. The results are reported in Figure 3. The surface complexation model of proton adsorption, as already mentioned, is a general model and, it is not intended to provide a detailed representation of the actual chemical reactions taking place at the solid-liquid interface. However, it has proven to be suitable for reproducing the experimental titration data observed for the investigated sediments. This was confirmed by the excellent agreement with experimental data, with a root mean square error (RMSE) of 0.068 pH units.

A procedure for calibration of parameters of Equation 7 was developed, in order to estimate electroosmotic flow as a function of local pH and electric field conditions. These coefficients are usually calibrated through laboratory electrophoretic measurements. For example, Kim et al. [13] used the electrophoretic light scattering technique to measure the relation between pH and zeta potential. Conversely, we estimated this relation from electroosmotic flow measurements during electrokinetic tests. The advantage of this approach is that electroosmotic properties are estimated in the actual conditions of ionic strength and fluid composition developed during the application of the electric field. Moreover, the measurements are performed with compacted soil rather than a suspension as they are for electrophoretic measurements. To estimate the ζ-pH relationship we assumed an exponential relation (Equation 7). Then, Equation 8 was used to estimate electroosmotic flow, using measured pH and electric field values as inputs to both equations. The parameters a, b and c in Equation 7 were chosen in order to minimize the discrepancy between electroosmotic flows observed and predicted by Equation 8. Being sediment pH determination a destructive measurement, it was only done at the beginning and at the end of each experiment (in five locations), for a total of 30 pH measurements. Therefore, the data available for calibration and validation were limited to measurements performed at the beginning and end of each test, for a total of 6 electroosmotic flow quantifications, 30 pH measurements and 30 electric field values. Data were split into two subsets; data measured during experiment 1 and 2 were used to calibrate the parameters and data from experiment 3 to validate the results. Regardless of the limited amount of data, the procedure produced excellent results as shown in Figure 4. Figure 4a compares observed and estimated electroosmotic flows. The divergence from the 1:1 line is minimum, and the RMSE is low as 0.28 ml day^{-1} (maximum error less than 2%). Figure 4b shows the shape of the fitted ζ-pH function. The calibrated parameters are reported in Table 6.

The voltage drop was monitored during the experiments in 6 locations. Figure 5 shows the voltages measured during EXP3, with the anode located at the left-hand side of the figure. As shown, the voltage drop was not constant with time, particularly in the zone near the anode. In this sediment portion, the voltage raised in the first 15 days and than decreased constantly until the end of the experiment. We attribute these variations to both the varying composition and ionic strength of the electrolyte and to the geochemical modifications induced by the incoming H^+ from the anode. These modifications might have altered surface

conductivity, porosity and tortuosity in the sections where the sediment is more affected by the incoming acid front. However, we believe that these limited changes in voltage gradient could be neglected and a constant voltage can be assumed in the model (Figure 5) with minor effects on model results. Nevertheless, both assumptions could be considered acceptable, given the good agreement with data shown in the next section.

3.3. Numerical simulation results

Figure 6 compares predicted and experimental pH profiles. H^+ produced at the anode generated an acid front which moved toward the cathode and progressively acidified the sediment. This process enabled the desorption of contaminants from the solid matrix. Overall, a good agreement with experimental data was observed. The slight disagreement in the anodic region for the 32 and 63 day experiments might be due to the constant voltage and local equilibrium assumptions. The better agreement verified on the long term pH profile (120 days) enabled to conclude that the local equilibrium assumption has a stronger impact than the constant voltage assumption. In fact, in accordance with Villen-Guzman et al. [43], pH-buffering process is kinetically controlled and might be a slow process especially in high buffering capacity soils. Accordingly, the effects of neglecting the kinetics of this process are particularly evident in short-term pH profiles. Consequently, acid front positions were not accurately predicted (32 and 63 days) but pH values were consistent with measured values.

Figure 7 compares electroosmotic flow prediction and validation (EXP3). It shows an excellent agreement between model and experiments. An inversion of electroosmotic flow direction was observed after about 30 days, which was attributed to sediment pH variation. Along with pH change due to acid front advance from the anode, the zeta potential of sediment particles changed, producing variations in electroosmotic flow magnitude and direction. According to the ζ-pH relationship fitted to experimental data (Figure 4b), the pH corresponding to the point of zero charge (PZC) of the investigated sediment was particularly high and it was estimated to be pH 7.59. In fact, as shown in Figure 6, after 30 days sediment pH was in the range 6.3-7.8. When this pH was achieved, the electroosmotic flow reached its

minimum and remained almost at zero for other 20-30 days, with small oscillations possibly due to the fluctuations around the PZC or pH heterogeneities. After 60 days, a progressive increase of electroosmotic flow intensity was observed in the opposite direction, (cathode to anode), due to the decreasing pH. These results show the good prediction of pH with time and the prediction capability of the calibrated ζ-pH relationship.

The investigated heavy metals (Pb, Zn and Ni) were transported by either electromigration or electroosmosis toward the electrodes. The transport of species with higher valence (e.g. Pb^{2+}, Ni^{2+}, $PbCl_4^{2-}$, etc.) was more influenced by electromigration, while the transport of zerovalent complexes occurred only by electroosmosis.

Figure 8 shows the predicted and observed heavy metal profiles as a function of the distance from the anode side, which is located at the left of the graphs. The three experimental profiles are very similar, showing a strong dependence on pH profiles (simultaneous lowering of pH and metal concentrations is always observed). Concentration peaks are observed near the cathode in the 63-day profile at about 20 cm from the anodic side, due to the accumulation of metals transported toward the cathode and immobilized in the cathodic region due to higher pH. The peaks progressively moved toward the cathode (120-day profiles) and then disappeared (180-day profiles).

The simulated Zn and Ni profiles are very close because model parameters defined for both species were similar. In fact, diffusion coefficients for Zn and Ni are comparable (Table 4), the parameters defined in the thermodynamic database are similar and the same type of aqueous complexes are formed. Moreover, the same linear distribution coefficient was used for both species.

Overall, the profiles were predicted with good accuracy. An overestimation of the removal was observed in the regions close to the anode (left-hand side). This could be due to metal bonding forms in the sediment. Taking into account heavy metal speciation in the investigated sediment (Table 2), the residual fraction (less mobile fraction) is of relevant importance. As a result, the metal concentration in the sediment could hardly be reduced to zero due to higher resilience of this fraction to the acid front.

Table 7 compares observed and predicted removal percentages. The highest removal was observed for Pb. This can be interpreted as a consequence of the lower Pb associated to the

residual fraction than Zn and Ni. Pb residual fraction was quantified as 20%, while values of 46.7% and 50.8% were found for Zn and Ni, respectively. These data correlate well with measured recoveries, observing that higher residual fraction resulted in lower overall metal removal.

The observed removal rates for Pb and Ni were well predicted and it was estimated that removal of 84.6% of Pb and 79.3% of Ni, respectively, would be achieved applying the treatment for 240 days in the same conditions. Anoverestimation for Zn removal rate was observed. This result was influenced by the high concentration measured near the cathode in the 63-day profile and the inconsistent concentration verified in the section close to the anode in which an increase of Zn was observed in the 120-day profile. The behaviour of Zn may be different from Pb and Ni due to the significantly higher initial content in the sediment.

4. Conclusions

We implemented a numerical model able to simulate transport of multiple species and geochemical reactions occurring during the remediation of real contaminated sediments characterized by a heterogeneous solid matrix and aged pollution. We identified the acid buffering capacity as the most significant factor for the extraction of heavy metals from the sediments as their speciation and mobility are strictly dependent on sediment capacity to hinder the pH shift to the acidic range. The main phenomena considered in the model, selected on the basis of literature review and laboratory experiments specifically carried out, were: (1) chemical species transport through the porous matrix by electromigration and electroosmosis, (2) pH-dependent adsorption of H^+ modelled as a general surface complexation reaction with equilibrium constants fitted to batch test data, (3) adsorption of contaminants onto sediment particle surfaces modelled as linear adsorption isotherms, (4) aqueous speciation and (5) formation/dissolution of solid precipitates. A constitutive relationship between zeta potential and pH was used to compute the local electroosmotic permeability. The electroosmotic flow was computed by volume averaging the electroosmotic permeability.

To validate the model, simulations were performed to reproduce the results of laboratory scale electrokinetic tests, carried out with different treatment durations (32, 63 and 120 days).

The calibration of model parameters was carried out through either batch tests and the outcome of the electrokinetic tests, separating calibration from validation data.

A good agreement was found between experimental data and model predictions. In particular, pH and electroosmotic flow were predicted with good accuracy. The predicted metal profiles were also close to experimental profiles for all of the investigated metals (Pb, Zn and Ni) but an overestimation of the removal was observed in the regions close to the anode, possibly due to the high residual fraction identified by sequential extraction.

The predicted removal efficiencies were in very good accordance with observed removal percentages for Pb and Ni and moderately overestimated for Zn. These results encourage the use of the model and of the modelling approach as an engineering tool for prediction of remediation efficiency for the design and practical implementation of electrokinetic technology at the field scale.

Acknowledgements

This work was financially supported by European Commission within the Life+ project LIFE12 ENV/IT/442 SEKRET “Sediment electrokinetic remediation technology for heavy metal pollution removal”. Authors wish to acknowledge Industrie De Nora s.p.a. for providing coated titanium electrodes and SGL Group for providing graphite rod electrodes. The authors are thankful to the anonymous reviewers for their valuable comments and suggestions that helped to improve the quality of the manuscript.

References

[1] C.N. Mulligan, R.N. Yong, B.F. Gibbs, An evaluation of technologies for the heavy metal remediation of dredged sediments, J. Hazard. Mater. 85 (2001) 145–163. doi:10.1016/S0304-3894(01)00226-6.

[2] J.-F. Peng, Y.-H. Song, P. Yuan, X.-Y. Cui, G.-L. Qiu, The remediation of heavy metals contaminated sediment., J. Hazard. Mater. 161 (2009) 633–40. doi:10.1016/j.jhazmat.2008.04.061.

[3] F. Rozas, M. Castellote, Electrokinetic remediation of dredged sediments polluted with heavy metals with different enhancing electrolytes, Electrochim. Acta. 86 (2012) 102–109. doi:10.1016/j.electacta.2012.03.068.

[4] R. Iannelli, M. Masi, A. Ceccarini, M.B. Ostuni, R. Lageman, A. Muntoni, D. Spiga, A. Polettini, A. Marini, R. Pomi, Electrokinetic remediation of metal-polluted marine sediments: experimental investigation for plant design, Electrochim. Acta. 181 (2015) 146–159. doi:10.1016/j.electacta.2015.04.093.

[5] A. Colacicco, G. De Gioannis, A. Muntoni, E. Pettinao, A. Polettini, R. Pomi, Enhanced electrokinetic treatment of marine sediments contaminated by heavy metals and PAHs., Chemosphere. 81 (2010) 46–56. doi:10.1016/j.chemosphere.2010.07.004.

[6] Y. Song, M.-T. Ammami, A. Benamar, S. Mezazigh, H. Wang, Effect of EDTA, EDDS, NTA and citric acid on electrokinetic remediation of As, Cd, Cr, Cu, Ni, Pb and Zn contaminated dredged marine sediment, Environ. Sci. Pollut. Res. (2016) 1–10. doi:10.1007/s11356-015-5966-5.

[7] Y.B. Acar, A.N. Alshawabkeh, Principles of electrokinetic remediation, Environ. Sci. Technol. 27 (1993) 2638–2647. doi:10.1021/es00049a002.

[8] A.T. Yeung, Y.-Y. Gu, A review on techniques to enhance electrochemical remediation of contaminated soils., J. Hazard. Mater. 195 (2011) 11–29. doi:10.1016/j.jhazmat.2011.08.047.

[9] A.N. Alshawabkeh, Electrokinetic Soil Remediation: Challenges and Opportunities, Sep. Sci. Technol. 44 (2009) 2171–2187. doi:10.1080/01496390902976681.

[10] A. Alshawabkeh, Y. Acar, Electrokinetic Remediation. II: Theoretical Model, J. Geotech. Eng. 122 (1996) 186–196. doi:10.1061/(ASCE)0733-9410(1996)122:3(186).

[11] J.M. Paz-Garcia, K. Baek, I.D. Alshawabkeh, A.N. Alshawabkeh, A generalized model for transport of contaminants in soil by electric fields, J. Environ. Sci. Heal. Part A. 47 (2012) 308–318. doi:10.1080/10934529.2012.640911.

[12] S. Amrate, D.E. Akretche, Modeling EDTA enhanced electrokinetic remediation of lead contaminated soils., Chemosphere. 60 (2005) 1376–83. doi:10.1016/j.chemosphere.2005.02.021.

[13] S.-O. Kim, J.-J. Kim, S.-T. Yun, K.-W. Kim, Numerical and Experimental Studies on Cadmium (II) Transport in Kaolinite Clay under Electrical Fields, Water. Air. Soil Pollut. 150 (2003) 135–162. doi:10.1023/A:1026181800685.

[14] J.-W. Yu, I. Neretnieks, Modelling of transport and reaction processes in a porous medium in an electrical field, Chem. Eng. Sci. 51 (1996) 4355–4368. doi:10.1016/0009-2509(96)00283-7.

[15] Y.S. Choi, R. Lui, A mathematical model for the electrokinetic remediation of contaminated soil, J. Hazard. Mater. 44 (1995) 61–75. doi:10.1016/0304-3894(95)00049-Z.

[16] R.A. Jacobs, M.Z. Sengun, R.E. Hicks, R.F. Probstein, Model and experiments on soil remediation by electric fields, J. Environ. Sci. Heal. . Part A Environ. Sci. Eng. Toxicol. 29 (1994) 1933–1955. doi:10.1080/10934529409376157.

[17] J.M. Paz-García, B. Johannesson, L.M. Ottosen, A.B. Ribeiro, J.M. Rodríguez-Maroto, Modeling of electrokinetic processes by finite element integration of the Nernst–Planck–Poisson system of equations, Sep. Purif. Technol. 79 (2011) 183–192. doi:10.1016/j.seppur.2011.02.023.

[18] E.D. Mattson, R.S. Bowman, E.R. Lindgren, Electrokinetic ion transport through unsaturated soil: 1. Theory, model development, and testing, J. Contam. Hydrol. 54 (2002) 99–120. doi:10.1016/S0169-7722(01)00144-9.

[19] J.M. Paz-García, M. Villén-Guzmán, A. García-Rubio, S. Hall, M. Ristinmaa, C. Gómez-Lahoz, A Coupled Reactive-Transport Model for Electrokinetic Remediation, in: A.B. Ribeiro, E.P. Mateus, N. Couto (Eds.), Electrokinet. Across Discip. Cont. SE - 13, Springer International Publishing, 2016: pp. 251–278. doi:10.1007/978-3-319-20179-5_13.

[20] A. Al-Hamdan, K. Reddy, Electrokinetic Remediation Modeling Incorporating Geochemical Effects, J. Geotech. Geoenvironmental Eng. 134 (2008) 91–105. doi:10.1061/(ASCE)1090-0241(2008)134:1(91).

[21] M. Mascia, A. Vacca, S. Palmas, Effect of surface equilibria on the electrokinetic behaviour of Pb and Cd ions in kaolinite, J. Chem. Technol. Biotechnol. 90 (2015) 1290–1298. doi:10.1002/jctb.4435.

[22] D.L. Parkhurst, C. a. J. Appelo, Description of Input and Examples for PHREEQC Version 3 — A Computer Program for Speciation , Batch-Reaction , One-Dimensional Transport , and Inverse Geochemical Calculations Chapter 43 of, in: U.S. Geol. Surv. Tech. Methods, B. 6, U.S. Geological Survey (USGS), 2013: p. 497.

[23] J.-W. Yu, I. Neretnieks, Theoretical evaluation of a technique for electrokinetic decontamination of soils, J. Contam. Hydrol. 26 (1997) 291–299. doi:10.1016/S0169-7722(96)00076-9.

[24] A.N. Alshawabkeh, Y.B. Acar, Removal of contaminants from soils by electrokinetics: A theoretical treatise, J. Environ. Sci. Heal. . Part A Environ. Sci. Eng. Toxicol. 27 (1992) 1835–1861. doi:10.1080/10934529209375828.

[25] C. Shackelford, D. Daniel, Diffusion in Saturated Soil. I: Background, J. Geotech. Eng. 117 (1991) 467–484. doi:10.1061/(ASCE)0733-9410(1991)117:3(467).

[26] G.R. Eykholt, D.E. Daniel, Impact of System Chemistry on Electroosmosis in Contaminated Soil, J. Geotech. Eng. 120 (1994) 797–815. doi:10.1061/(ASCE)0733-9410(1994)120:5(797).

[27] L. Casagrande, Electro-Osmosis in Soils, Géotechnique. 1 (1949) 159–177. doi:10.1680/geot.1949.1.3.159.

[28] J.-S. Park, S.-O. Kim, K.-W. Kim, B.R. Kim, S.-H. Moon, Numerical analysis for electrokinetic soil processing enhanced by chemical conditioning of the electrode reservoirs, J. Hazard. Mater. 99 (2003) 71–88. doi:10.1016/S0304-3894(03)00038-4.

[29] D.A. Dzombak, F.M.M. Morel, Surface complexation modeling: hydrous ferric oxide, John Wiley & Sons, 1990.

[30] A. Al-Hamdan, K. Reddy, Surface Speciation Modeling of Heavy Metals in Kaolin: Implications for Electrokinetic Soil Remediation Processes, Adsorption. 11 (2005)

529–546. doi:10.1007/s10450-005-5611-6.

[31] W. Stumm, J.J. Morgan, Aquatic Chemistry: Chemical Equilibria and Rates in Natural Waters, Third edit, Wiley-Interscience, 1995. doi:10.1016/S0016-7037(97)81133-7.

[32] J.A. Davis, J.A. Coston, D.B. Kent, C.C. Fuller, Application of the Surface Complexation Concept to Complex Mineral Assemblages, Environ. Sci. Technol. 32 (1998) 2820–2828. doi:10.1021/es980312q.

[33] B.D.L. Parkhurst, C. a J. Appelo, User's Guide To PHREEQC (version 2) — a Computer Program for Speciation, Batch-Reaction, One-Dimensional Transport and Inverse Geochemical Calculations, 1999. http://downloads.openchannelsoftware.org/PHREEQC/manual.pdf.

[34] M.Z. Wu, D.A. Reynolds, H. Prommer, A. Fourie, D.G. Thomas, Numerical evaluation of voltage gradient constraints on electrokinetic injection of amendments, Adv. Water Resour. 38 (2012) 60–69. doi:10.1016/j.advwatres.2011.11.004.

[35] H.I. Gomes, J.M. Rodríguez-Maroto, A.B. Ribeiro, S. Pamukcu, C. Dias-Ferreira, Numerical prediction of diffusion and electric field-induced iron nanoparticle transport, Electrochim. Acta. 181 (2015) 5–12. doi:10.1016/j.electacta.2014.11.157.

[36] J. Carrayrou, R. Mosé, P. Behra, Operator-splitting procedures for reactive transport and comparison of mass balance errors., J. Contam. Hydrol. 68 (2004) 239–68. doi:10.1016/S0169-7722(03)00141-4.

[37] E.J.F. Dickinson, H. Ekström, E. Fontes, COMSOL Multiphysics®: Finite element software for electrochemical analysis. A mini-review, Electrochem. Commun. 40 (2014) 71–74. doi:10.1016/j.elecom.2013.12.020.

[38] D.L. Parkhurst, L. Wissmeier, PhreeqcRM: A reaction module for transport simulators based on the geochemical model PHREEQC, Adv. Water Resour. 83 (2015) 176–189. doi:10.1016/j.advwatres.2015.06.001.

[39] M. Masi, R. Iannelli, G. Losito, Ligand-enhanced electrokinetic remediation of metal-contaminated marine sediments with high acid buffering capacity, Environ. Sci. Pollut. Res. 23 (2016) 10566–10576. doi:10.1007/s11356-015-5563-7.

[40] J. Newman, K.E. Thomas-Alyea, Electrochemical Systems, Wiley, 2012. http://books.google.it/books?id=eyj4MRa7vLAC.

[41] K.R. Reddy, C. Cameselle, Electrochemical Remediation Technologies for Polluted Soils, Sediments and Groundwater, Wiley, 2009.

[42] J.D. Allison, D.S. Brown, J. Kevin, MINTEQA2/PRODEFA2, a geochemical assessment model for environmental systems: Version 3.0 user's manual, Environmental Research Laboratory, Office of Research and Development, US Environmental Protection Agency Athens, GA, 1991.

[43] M. Villen-Guzman, J.M. Paz-Garcia, G. Amaya-Santos, J.M. Rodriguez-Maroto, C. Vereda-Alonso, C. Gomez-Lahoz, Effects of the buffering capacity of the soil on the mobilization of heavy metals. Equilibrium and kinetics., Chemosphere. 131 (2015) 78–84. doi:10.1016/j.chemosphere.2015.02.034.

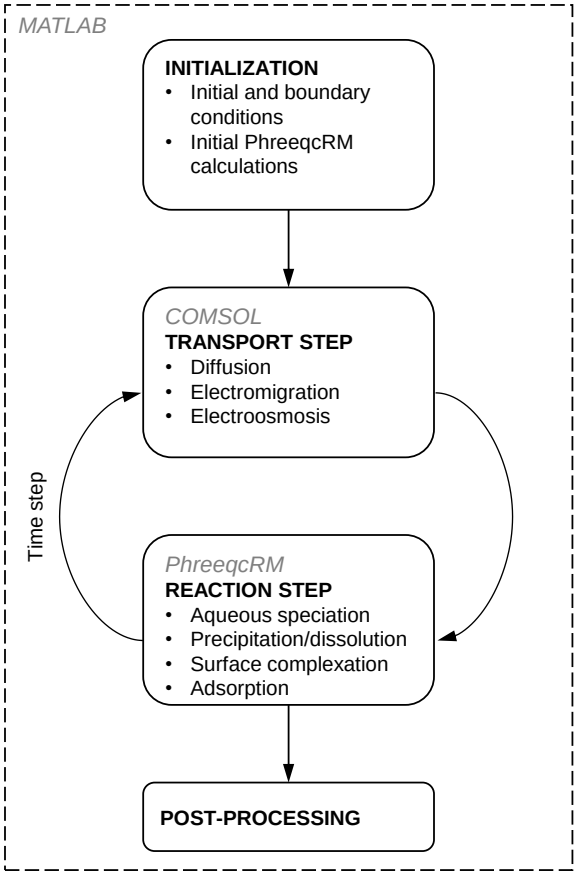

Figure 1. Numerical implementation structure of the reactive-transport model

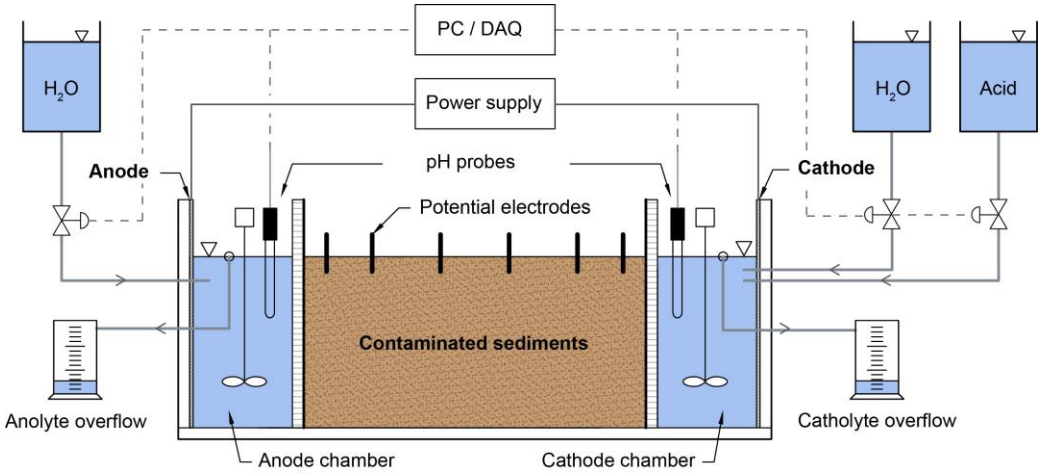

Figure 2. Experimental setup for electrokinetic remediation tests

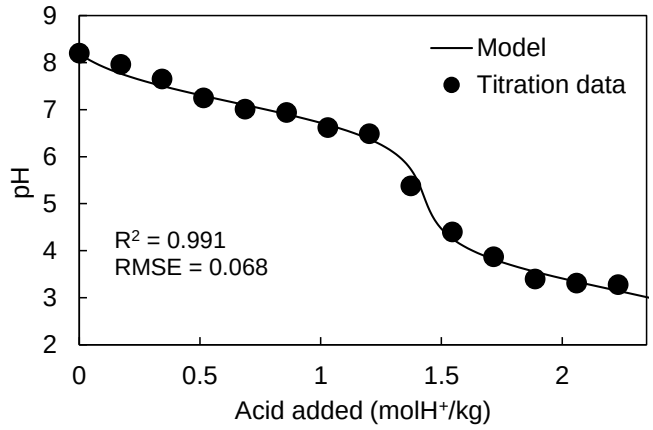

Figure 3. Fitting of surface complexation model to experimental titration data

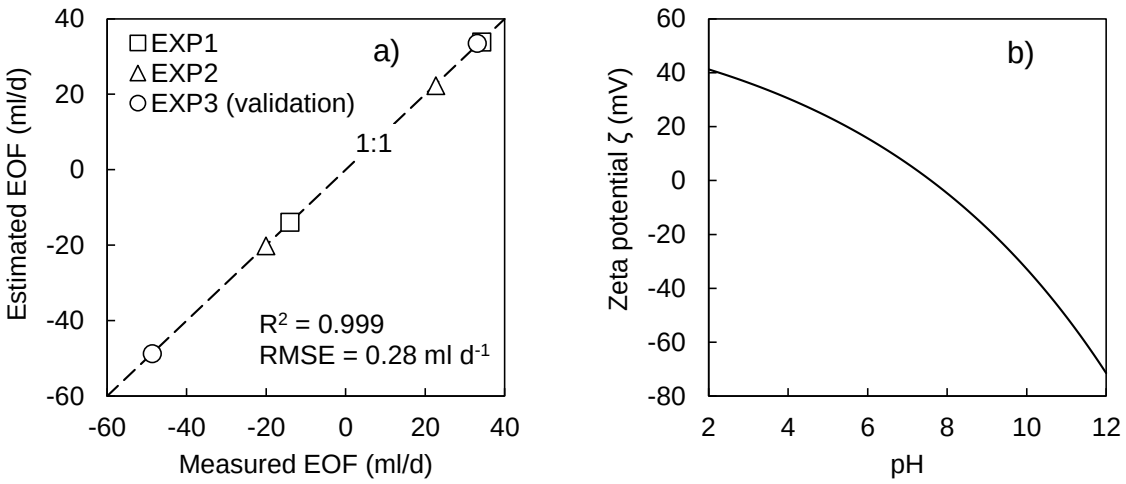

Figure 4. a) Comparison between electroosmotic flow (EOF) measured and estimated with Equation 8. b) ζ-pH relationship (Equation 7) with calibrated parameters

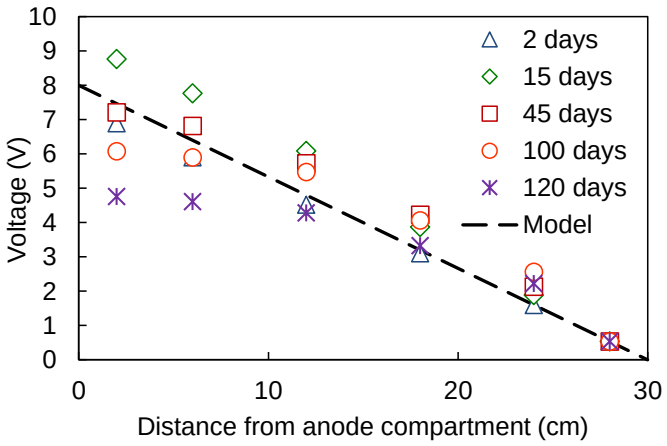

Figure 5. Electrical potential distribution measured during EXP3 and voltage profile set in the model

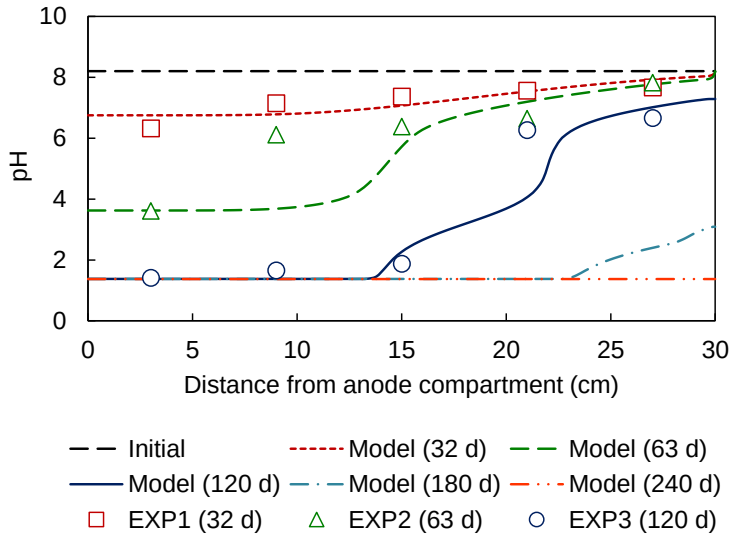

Figure 6. Predicted and measured pH profiles. Error bars are not shown because the measured error over three replicates was less than 0.2 pH units

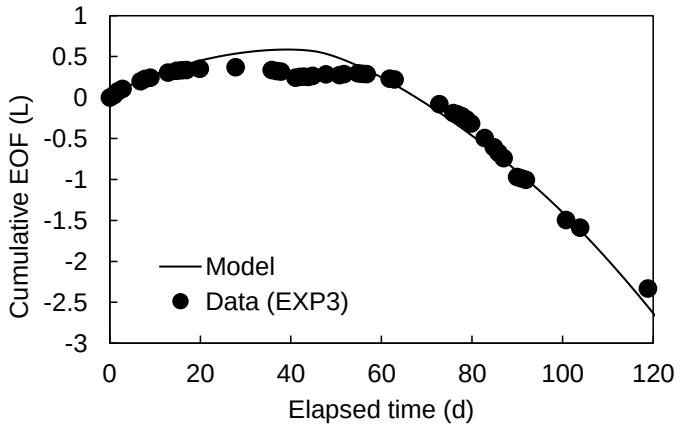

Figure 7. Comparison between predicted and measured electroosmotic flow (EOF)

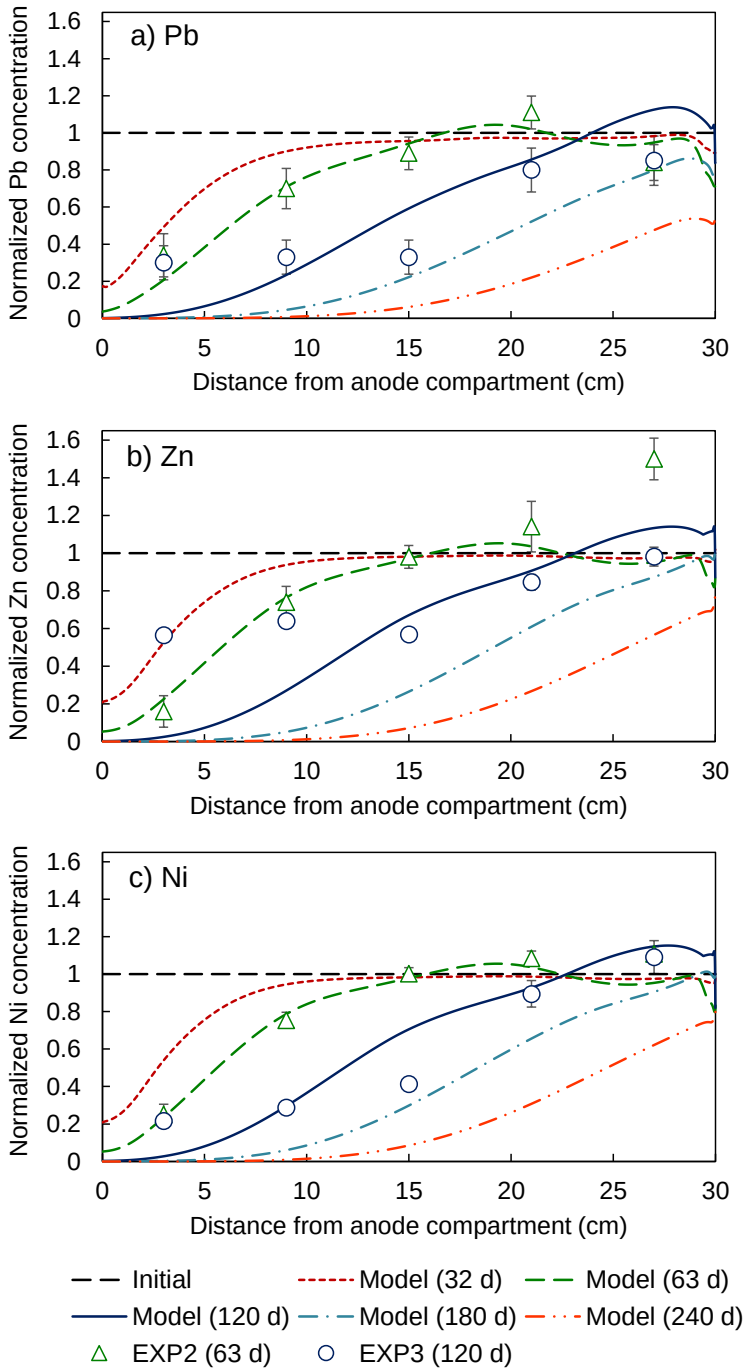

Figure 8. Model predictions and experimental profiles of Pb, Zn and Ni. Error bars are calculated over three replicates

Table 1. Physicochemical properties of the sediments and metal content

Property	**Value**
Particle size distribution:	
Coarse and medium sand	25.70 %
Fine sand	25.40 %
Silt	18.00 %
Clay	30.90 %
Porosity	0.52 ± 0.05
Hydraulic conductivity	3.7×10^{-10} m/s
Moisture	31.9 ± 1.3 %
pH	8.32 ± 0.14
Buffering capacity:	
to pH = 3 ± 0.2	2.36 mol H^+/kg
to pH = 13 ± 0.2	0.78 mol OH^-/kg
Electrical resistivity	0.55 ± 0.1 Ωm
Pore water conductivity	52 ± 5 mS/cm
Cation exchange capacity (CEC)	11.2 ± 0.9 meq/100 g
Total Organic Carbon (TOC)	< 0.5 %
Metal content:	
Pb	67.2 ± 19.4
Zn	893.2 ± 289.2
Ni	50.5 ± 12.4
Cu	522 ± 158.4
Cd	1.33 ± 0.15

Table 2. Heavy metal speciation in the untreated sediments

Fraction	**Pb**	**Zn**	**Ni**
Exchangeable (%)	5.9	19.1	9.7
Reducible (%)	56.1	20.9	16.3
Oxidisable (%)	17.9	13.3	23.2
Residual (%)	20.0	46.7	50.8

Table 3. Experimental conditions for electrokinetic treatments.

Test	Duration (days)	Applied current density (A/m^2)	Anolyte	Catholyte
EXP1	32	40	Deionized water	HNO_3
EXP2*	63	40	Deionized water	HNO_3
EXP3	120	40	Deionized water	HNO_3

* Experimental results from Iannelli et al. [4]

Table 4. Diffusion coefficients of modelled species at infinite dilution

Species	**D (m^2/s)**
H^+	9.312×10^{-9}
OH^-	5.260×10^{-9}
Na^+	1.334×10^{-9}
Cl^-	2.032×10^{-9}
NO_3^-	1.902×10^{-9}
Pb^{2+}, $PbCl^+$, $PbCl_3^-$, $PbCl_4^{2-}$, $PbCl_2$, $PbNO_3^+$, $Pb(NO_3)_2$	9.25×10^{-10}
Zn^{2+}, $ZnCl^+$, $ZnCl_3^-$, $ZnCl_4^{2-}$, $ZnCl_2$, $ZnNO_3^+$	7.02×10^{-10}
Ni^{2+}, $NiCl^+$, $NiNO_3^+$	6.79×10^{-10}

Table 5. Initial conditions

Species	Initial concentration (M)
H^+	$10^{-8.2}$
OH^-	From equilibrium
Na^+	0.5
Cl^-	0.5
NO_3^-	10^{-3}
Pb^{2+}	1.07×10^{-3}
Zn^{2+}	4.52×10^{-2}
Ni^{2+}	2.85×10^{-3}

Table 6. Model parameters

Parameter	**Value**	**Unit**	**Description**
τ	0.80	-	Tortuosity factor
n	0.52	-	Porosity
a	69.76	mV	Parameter Eq. 7
b	–20.71	-	Parameter Eq. 7
c	0.15 ± 0.02	-	Parameter Eq. 7
J	40	A/m^2	Current density
V_{AN}	8	V	Voltage at the anode
V_{CAT}	0	V	Voltage at the cathode
T	25	°C	Temperature
$\log(K_{d,Pb})$	2.7	-	Pb distribution coeff.
$\log(K_{d,Zn})$	2.4	-	Zn distribution coeff.
$\log(K_{d,Ni})$	2.4	-	Ni distribution coeff.
Reactions	**log(K)**		
$\equiv SOH + H^+ \rightleftharpoons \equiv SOH_2^+$	3.18		Protonation reaction
$\equiv SOH \rightleftharpoons \equiv SO^- + H^+$	–7.14		Deprotonation reaction

Table 7. Observed and predicted removal efficiencies (%)

	EXP2 - 63 days		EXP3 - 120 days		Model prediction
	Observed	**Predicted**	**Observed**	**Predicted**	**240 days**
Pb	22.3	24.3	47.8	43.8	84.6
Ni	16.0	20.6	41.9	38.2	79.3
Zn	9.5	21.4	28.0	40.1	81.5